Heteronuclear soliton molecules with two frequencies

Stephanie Willms,[1,2] Oliver Melchert,[1,2,3] Surajit Bose,[1,2] Alexey Yulin,[4] Ivan Oreshnikov,[5] Uwe Morgner,[1,2,3] Ihar Babushkin,[1,2] and Ayhan Demircan[1,2,3]

[1]*Cluster of Excellence PhoenixD, Leibniz Universität Hannover, Welfengarten 1, 30167 Hannover, Germany*
[2]*Institute of Quantum Optics, Leibniz Universität Hannover, Welfengarten 1, 30167 Hannover, Germany*
[3]*Hannover Centre for Optical Technologies, Leibniz Universität Hannover, Nienburger Straße 17, 30167 Hannover, Germany*
[4]*Department of Nanophotonics and Metamaterials, ITMO University, 197101 Saint Petersburg, Russia*
[5]*Max Planck Institute for Intelligent Systems, Max-Planck-Ring 4, 72076 Tübingen, Germany*

(Received 29 July 2021; revised 18 March 2022; accepted 11 May 2022; published 27 May 2022)

Bound states of optical solitons represent ideal candidates to investigate fundamental nonlinear wave interaction principles and have been shown to exhibit intriguing analogies to phenomena in quantum mechanics. Usually, such soliton molecules are created by a suitable balance of phase-related attraction and repulsion between two copropagating solitons with overlapping tails. However, there exists also another type of compound state, where strong binding forces result directly from the Kerr nonlinearity between solitons at different center frequencies. The physical mechanisms as well as the properties of these objects are quite different from those of usual soliton molecules, but are hardly known. Here we characterize and investigate these compound states in greater detail. We demonstrate unique propagation dynamics by investigating the robustness of the compound states under perturbations, such as third-order dispersion and the Raman effect. The constituents are individually affected by the perturbations, but the impact on the compound state is not a mere superimposition. One observes complex dynamics resulting from a strong entanglement between the subpulses. For example, in the case of the Raman effect both subpulses are subject to a cancellation of the self-frequency shift, although only one subpulse is approaching a zero-dispersion frequency. We extend the concept of the molecule states to three and more constituents by adopting appropriate propagation constants. These multicolor soliton molecules open up further perspectives for exploring the complex physics of photonic molecules, but also show great potential for application resulting from their robustness and the possibility to control their properties.

DOI: 10.1103/PhysRevA.105.053525

I. INTRODUCTION

Solitons are localized wave solutions of the nonlinear Schrödinger equation (NLSE) enabled by the interplay of nonlinear and dispersive effects [1,2]. Their stable propagation without changing their shape makes them ubiquitous objects in different areas of science [3,4], especially in nonlinear optics [5–7]. Optical solitons are often associated with a particlelike behavior that manifests itself via complex soliton-soliton interactions like collisions [8] or trapping [9]. Bound states of two or more solitons can also be understood as an extension of the concept of quantum-mechanical particles to a compound of particles. These soliton molecules appear throughout different physical systems, e.g., in dispersion-managed fibers where they are defined by a characteristic double-hump structure in the time domain [10,11]. Such temporal pulse compounds appear in nonlinear optical fibers governed by the generalized NLSE [12], the dissipatively perturbed NLSE [13], coupled NLSEs describing twin-core fibers [14], or the complex Ginzburg-Landau equation [15,16]. Soliton molecules also exist in microresonators that support dissipative Kerr solitons [17]. Similar pulse compounds also appear in other contexts [18–28]. The common feature of these soliton molecules is that their constituent subpulses are stable units themselves. Therefore, the subpulses can propagate stably also when they are separated from their binding partner. The binding mechanism of these molecules is based on the phase relation between the bound subpulses.

Recently, a fundamentally different kind of soliton molecule was demonstrated [29], here referred to as a two-frequency soliton molecule or two-frequency pulse compound. Such molecule states have also been investigated as a part of a larger class of generalized dispersion Kerr solitons in [30]. Therein, they are described for a nonlinear Schrödinger equation with positive quadratic and negative quartic dispersion. For these dispersion conditions, molecule states were recently observed experimentally in a mode-locked laser cavity for the first time [31], where an enhanced effective nonlinear parameter for the compound state was discussed. Two-color soliton microcomb states with a similar pulse structure were also observed in microresonators modeled by the Lugiato-Lefever equation [32,33]. In contrast to usual soliton molecules, which exhibit a double-hump structure in the time domain, these molecules are characterized by a double-hump structure in the frequency domain where the two subpulses are located at vastly separated frequencies at which dispersion is anomalous. In the time domain the molecule state consists of a single localized state. The two

constituent subpulses have energies below that of fundamental solitons and deviate also from hyperbolic secant shapes. Stable propagation of the separated subpulses is not possible and a stable molecule exists only as an inseparable unit. The subpulses have different pulse durations, intensities, and frequencies. Since the constituents are therefore unequal, the resulting molecule can be considered to be heteronuclear [17]. To engage in a strong mutual interaction, both subpulses need similar group velocities. This requires a propagation constant that exhibits at least two domains of anomalous dispersion, enabling group-velocity-matched copropagation among the molecules subpulses. Suitable waveguides that fulfill these criteria exist, e.g., in microstructured fibers [34], silicon slot waveguides [35,36], or dispersion-manageable mode-locked laser cavities [31]. Group-velocity-matched interaction between a soliton and a dispersive wave, interacting across a single zero-dispersion point, was shown to give rise to a strong repulsion between both pulses [37–39]. In optics, the underlying mechanism is referred to as the optical push broom effect [40], optical event horizon [41,42], or temporal reflection [43], facilitating strong and efficient all-optical control of light by light [37,44,45].

For the case of two pulses in separated anomalous dispersion regimes such a cross-phase modulation (XPM)–based interaction is attractive and provides the binding mechanism for the soliton molecules [29]. In Ref. [46] we showed the robustness of the pulse compounds by investigating the influence of group-velocity mismatches of the initial solitons. This revealed a crossover behavior from the formation of two-frequency soliton molecules to escaping solitons. We also recently demonstrated that the resulting molecule states are independent of any phase relation [47]. Furthermore, the introduction of a simplified model for a special class of solutions allowed us to obtain analytic solutions for the molecule states, explaining the special energy relation within the molecule states mentioned above. However, this description holds only for solutions where the constituents are well separated and exclusively located in the anomalous dispersion regime. The general class of solutions exhibits much more complex characteristics with energy content ranging also over the normal dispersion regime. The characteristics of these states as well as their behavior under perturbation are yet unknown.

We study here heteronuclear two-color soliton molecules in further detail. We more closely look at the substructure of different molecule states and consider different means of molecule generation, discussing their influence on the resulting two-frequency pulse compounds. Going beyond previous works, we investigate how these molecules are affected by different types of perturbation, such as higher-order dispersion and the Raman effect. An important feature is that a perturbation of one individual subpulse influences also the second subpulse, due to their strong interconnection. Our system provides unique conditions concerning perturbations. The impact of third-order dispersion is guided by different signs for the subpulses and for the Raman effect one subpulse is subject to the spectral recoil [48] while the other is unaffected from a zero-dispersion point. The aim is to understand the impact these perturbations have on the propagation of the pulse compounds. Furthermore, we consider waveguides with three separate domains of anomalous dispersion. Within the presented framework, this allows us to extend the concept of moleculelike bound states of two pulses to mutually bound pulse triplets.

The remainder of the article is organized as follows. In Sec. II we detail the considered propagation model. We then discuss the characteristics and generation of two-frequency molecules in Sec. III A and Sec. III B and investigate their propagation dynamics under various perturbations in Sec. III C. In Sec. III D we extend the concept to support bound states of three pulses. We conclude with a summary in Sec. IV.

II. THEORETICAL MODEL

A common way to describe pulse propagation in waveguides is using the so-called generalized nonlinear Schrödinger equation (GNLSE) [49,50]. For our investigation, we use a first-order nonlinear propagation equation

$$i\partial_z\mathcal{E}_\omega + \Big(\beta(\omega) - \frac{\omega}{v_0} + i\alpha(\omega)\Big)\mathcal{E}_\omega + \frac{3\omega^2\chi}{8c^2\beta(\omega)}((1-f_R)|\mathcal{E}|^2\mathcal{E} + f_R\mathcal{I}_R\mathcal{E})_{\omega>0} = 0 \quad (1)$$

for the analytic signal $\mathcal{E}(z,t) = 2\sum_{\omega>0} E_\omega(z)e^{-i\omega t}$ [51,52], which inherently includes the GNLSE [53]. The real-valued field reads $E(z,t) = \sum_\omega E_\omega(z)e^{-i\omega t}$. Indices specify the domain and simplify the notation, e.g., $\mathcal{E}_\omega = \mathcal{E}(z,\omega)$ and $\mathcal{E} = \mathcal{E}(z,t)$. The χ refers to the third-order nonlinear susceptibility and c to the speed of light. The propagation constant is defined as $\beta(\omega) = \omega\,\mathrm{Re}[n(\omega)]/c$ [53,54], with $n(\omega)$ the frequency-dependent refractive index. To directly obtain the dynamics in a reference frame moving with velocity v_0, the propagation constant is modified to $\beta(\omega) - \omega/v_0$. Linear loss is modeled by the root-power attenuation $\alpha(\omega) = \omega\,\mathrm{Im}[n(\omega)]/c$. We find that for realistic values of $\alpha(\omega)$ it can be neglected for the propagation distances considered here. Further, the delayed Raman response is included as

$$\mathcal{I}_R = \sum_\omega \frac{\nu_1^2+\nu_2^2}{\nu_1^2-(\omega+i\nu_2)^2}(|\mathcal{E}|^2)_\omega e^{-i\omega t}, \quad (2)$$

with the parameters $\nu_1 = 0.082$ pHz and $\nu_2 = 0.031$ pHz, i.e., material-specific values for fused silica, and the fractional Raman contribution $f_R = 0.18$. As we will show below in Sec. III C, the Raman effect reveals new features regarding the propagation dynamics of molecule states. A suitable initial condition for Eq. (1), supporting the formation of a molecule state upon propagation, is the real-valued electric field

$$\sqrt{\chi}E(0,t) = \mathrm{Re}\left[\frac{N_1 a_1 e^{-i\omega_1 t}}{\cosh(t/t_1)} + \frac{N_2 a e^{-i\omega_2 t}}{\cosh[(t-\delta)/t_2]}\right] \quad (3)$$

with pulse durations $t_{1,2}$, center frequencies $\omega_{1,2}$, and soliton orders $N_{1,2}$. The electric field $E(z=0,t) = \sum_\omega E_\omega(z=0)e^{-i\omega t}$ is given in terms of a complex-valued analytic signal $\mathcal{E}(z=0,t) = 2\int_{\omega>0} d\omega\, E_\omega(z=0)e^{-i\omega t}$. Amplitudes of fundamental solitons read $a_{1/2} = \sqrt{|\beta_2(\omega_{1,2})|/t_{1,2}^2\gamma(\omega_{1,2})}$, with $\gamma(\omega_{1,2}) = 3\omega_{1,2}/8n(\omega_{1,2})c$ the frequency-dependent nonlinear coefficient. Equation (3) describes a superposition of two

solitons, where a direct initial overlap is realized for the pulse delay $\delta = 0$ fs.

Equation (1) is a nonlinear partial differential equation combining different higher-order linear terms and nonlinear terms [55,56]. The numerical investigation presented in this work is performed by a pseudospectral split-step routine, where the nonlinear part is solved by a Runge-Kutta scheme of fourth order [57]. It is convenient to use the Hamiltonian framework detailed in Ref. [53]. To this end, Eq. (1) is expressed in terms of the canonical variable by introducing

$$\mathcal{A}_\omega = \sqrt{|\beta(\omega)|/2\mu_0\omega^2}\mathcal{E}_\omega, \tag{4}$$

with μ_0 the permeability of free space. The Hamiltonian is given as

$$H = \sum_{\omega>0} \beta(\omega)|\mathcal{A}_\omega|^2 + \tfrac{3}{8}\sum_{1\bar{2}\bar{3}\bar{4}|} T^{(3)}_{1234}\mathcal{A}_{\omega_1}\mathcal{A}^*_{\omega_2}\mathcal{A}_{\omega_3}\mathcal{A}^*_{\omega_4}, \tag{5}$$

where

$$T^{(3)}_{1234} = \frac{\mu_0\chi|\omega_1\omega_2\omega_3\omega_4|}{c^2\sqrt{|\beta(\omega_1)\beta(\omega_2)\beta(\omega_3)\beta(\omega_4)|}}$$

and the sum index $1\bar{2}3\bar{4}|$ stands for the condition $\omega_1 - \omega_2 + \omega_3 - \omega_4 = 0$. The second term of Eq. (5) denotes the nonlinear interaction term $H_{\rm int}[\mathcal{A}]$. Following the ansatz discussed in [29], we can define the mutual interaction

$$H^{(12)}_{\rm int} = H_{\rm int}[\mathcal{A}] - (H_{\rm int}[\mathcal{A}_1] + H_{\rm int}[\mathcal{A}_2]) \tag{6}$$

for the self-interaction contributions $H_{\rm int}[\mathcal{A}_1]$ and $H_{\rm int}[\mathcal{A}_2]$ for the individual subpulses $\mathcal{A}_1(t) = \sum_{\omega<\omega_F}\mathcal{A}_\omega e^{-i\omega t}$ and $\mathcal{A}_2(t) = \sum_{\omega>\omega_F}\mathcal{A}_\omega e^{-i\omega t}$. The ω_F defines a suitable choice of a frequency separating the two subpulses in the frequency domain. Here we choose $\omega_F = 2$ rad/fs.

For the first investigation of the basic characteristics of the soliton molecule state without perturbation, we deliberately choose to neglect the Raman contribution. For Eq. (1) we can derive the conserved time-averaged energy flux [53]

$$\mathsf{E} = \sum_{\omega>0}\omega|\mathcal{A}_\omega|^2. \tag{7}$$

To describe two-frequency pulse compounds so that both time-domain and frequency-domain information is available simultaneously, we use the spectrogram

$$P_S(z,\tau,\omega) = \frac{1}{2\pi}\left|\int \mathcal{E}(z,t)h(t-\tau)e^{-i\omega t}dt\right|^2 \tag{8}$$

of the analytic signal $\mathcal{E}(z,t)$, using a hyperbolic secant $h(x) = \mathrm{sech}(x/\sigma)$ with width σ to localize the field in time [58].

In Fig. 1 dispersion characteristics are presented that fulfill the prerequisites of two-frequency molecule formation as mentioned before: a group-velocity-matched copropagation of the subpulses in separated regions of anomalous dispersion. The group-velocity $v_g = \beta_1^{-1}$ and group-velocity dispersion β_2 profiles are shown in Figs. 1(a) and 1(b), respectively. The group-velocity dispersion β_2 is shown for two of the three zero-dispersion frequencies (ZDFs) $(\omega_{Z1}, \omega_{Z2}, \omega_{Z3}) = (1.511, 2.511, 5.461)$ rad/fs that divide the angular frequency domain into two regions of anomalous dispersion (AD_1 and AD_2), separated by a normal dispersion region ND [gray shaded region in Fig. 1(b)]. The group-velocity-matched copropagation of light pulses in separate regions of anomalous dispersion can be realized within the shaded frequency ranges, highlighted in Fig. 1(a). Therein, two representative pairs of group-velocity-matched frequencies (ω_1, ω_2) are indicated. In either case, at both these frequencies, dispersion is anomalous [see Fig. 1(b)]. For the example of the pair labeled S_1 and S_2, the group-velocity-matched frequency in the interjacent region of normal dispersion is indicated by a square. Due to asymmetry of the propagation constant, group-velocity-matched pulses $[v_g(\omega_1) = v_g(\omega_2)]$ exhibit $\beta_2(\omega_1) \neq \beta_2(\omega_2)$. Also, as evident from Fig. 1(b), the slopes of β_2 at ω_1 and ω_2 are of different sign.

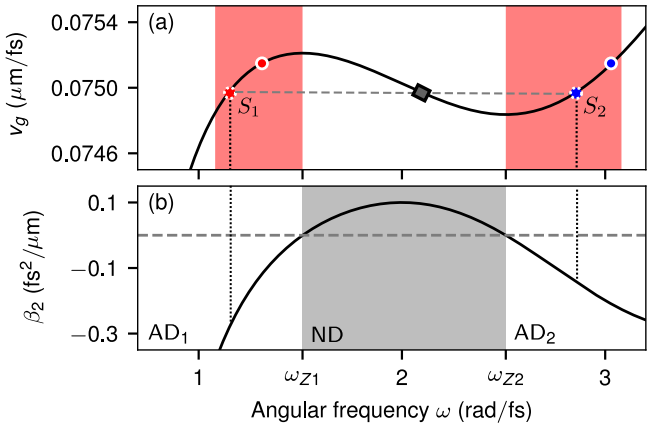

FIG. 1. Characteristics of the propagation constant. (a) Group-velocity (v_g) profile. Shaded areas indicate regions of possible group-velocity matching between anomalously dispersive pulses. Pairs of red and blue circles denote representative group-velocity-matched pairs of frequencies. For the pair labeled S_1 and S_2, the interjacent group-velocity-matched frequency at normal dispersion is marked by a square. (b) Group-velocity dispersion (β_2) profile. The shaded area indicates the region of normal dispersion (labeled ND). Black dotted lines indicate β_2 values for points S_1 and S_2.

For the following investigation we consider asymptotic molecule states which do not change anymore with further propagation. A molecule state separates after a certain propagation distance from radiation initially generated in the time domain. This radiation ejected during the transient creation process has a velocity different from that of the localized molecule state such that it can be separated distinctly into an asymptotic molecule and accompanying radiation [29]. We refer to this process as temporal filtering.

III. RESULTS

A. Characteristics of the soliton molecule

The important characteristic of the presented soliton molecules is the double-hump structure in the frequency domain. In Fig. 2 we demonstrate the influence of the initial conditions, such as pulse duration, on this fundamental property. We compare three different asymptotic molecule states, generated by a superposition of two group-velocity-matched solitons: the first one with an initial soliton pulse duration of $t_{1,2} = 100$ fs [light green line in Figs. 2(b) and 2(c)], the second with $t_{1,2} = 20$ fs [green line in Figs. 2(d) and 2(e)],

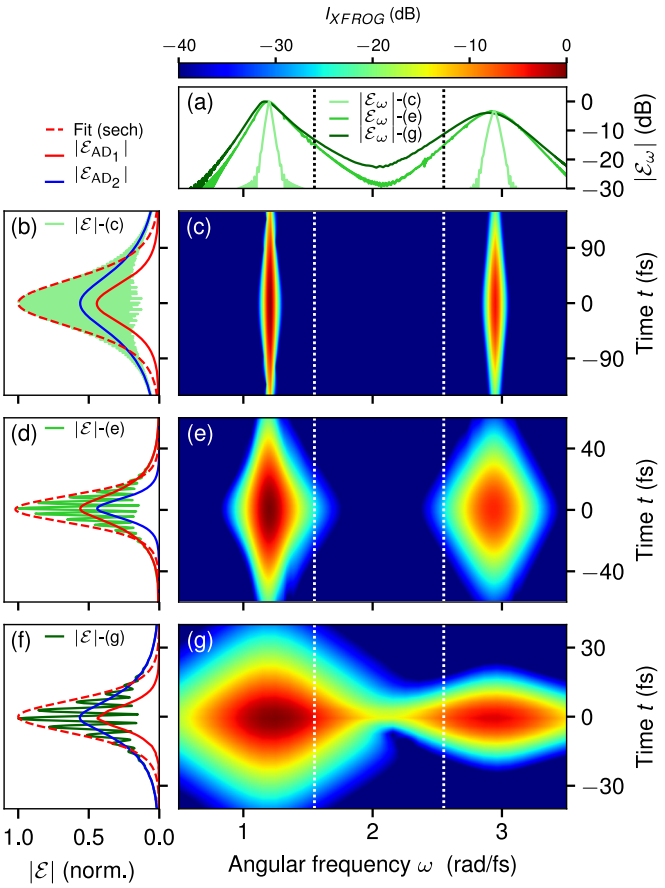

FIG. 2. Pulse characteristics of three different soliton molecules. (a) Spectra, (b) temporal profile, and (c) spectrogram with $\sigma = t_M$ of the molecule state generated by the superposition of two fundamental solitons with initial center frequencies $\omega_1 = 1.2$ rad/fs and $\omega_2 = 2.939$ rad/fs and pulse durations $t_{1,2} = 100$ fs. Subpulses in AD_1 and AD_2 are denoted by red and blue lines, respectively. The red dashed curve denotes a sech-shaped fit to the envelope. Panels (d) and (e) and panels (f) and (g) are the same as (b) and (c) but for molecules generated with (d) and (e) $t_{1,2} = 20$ fs and (f) and (g) $t_{1,2} = 15$ fs. The white and black dotted lines mark the position of the two ZDFs.

and the third with $t_{1,2} = 15$ fs [dark green line in Figs. 2(f) and 2(g)]. Their respective temporal profiles are shown in Figs. 2(b), 2(d), and 2(f), where the envelopes are fitted at best with a hyperbolic secant shape (red dashed line) with the pulse duration t_M of the respective asymptotic molecule state. The red and blue lines denote the temporal profiles of the subpulse in AD_1 and AD_2, respectively. Figure 2(a) compares the spectra of the molecule states. The two peaks of the first molecule state are well distinguishable. Also, the spectrogram in Fig. 2(c) shows no spectral energy in the region of normal dispersion ND. Instead, the second molecule ranges over the full spectrum shown [Fig. 2(a)] and the spectrogram [Fig. 2(e)] reveals an overlap of the constituents in the region of normal dispersion. This property becomes even more obvious for the third example in Figs. 2(f) and 2(g), where the contribution in the region of normal dispersion is not negligible. The fitting to a sech shape is very accurate in the region around the peak where the intensity is high, but

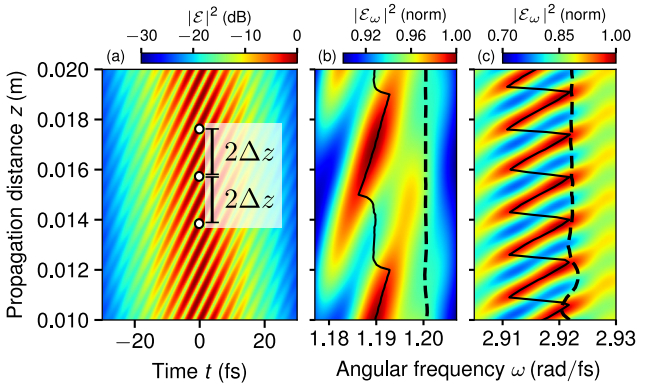

FIG. 3. Characterization of the molecule state. Evolution is shown in (a) the time and (b) and (c) the spectral domain. Circles mark positions where maxima appear with a periodicity of $2\Delta z$. Solid lines denote the position of the maximum in the spectral domain and dashed lines the positions of the frequency centroids ω_{1-C} and ω_{2-C}.

deviates for the pulse tails [see Figs. 2(b), 2(d), and 2(f)]. This results from the different values for, e.g., β_2 in the regions where the linear term dominates the nonlinear contribution such that the exponential tails deviate. The example demonstrated in Figs. 2(d) and 2(e) serves as an initial condition for most of the following investigation of this work. The molecule state has a contribution in the region ND, but yet two clearly distinguishable subpulses in the spectrum.

Figure 3 presents the evolution of the asymptotic two-frequency molecule state of Figs. 2(d) and 2(e). The z propagation of the intensity $|\mathcal{E}|^2$ in the time domain is shown in Fig. 3(a). The evolution of the subpulses in AD_1 and AD_2 is presented in Figs. 3(b) and 3(c), respectively. The evolution of the molecule state in the time domain is accompanied by interference fringes with the period $\Delta z \approx 0.098$ cm. To highlight the periodic pattern, circles have been added separated by a distance $2\Delta z$ to Fig. 3(a). Here each circle lies on an alternative maximum of the interference pattern. Furthermore, the evolution of the subpulses in the spectral domain reveals also a periodicity. The tracing of the maxima (solid line) highlights this behavior. Since an asymptotic molecule state is chosen, the amplitude of the oscillation of the subpulses maxima stays unchanged with ongoing propagation [29]. To demonstrate this, we show also the evolution of the frequency centroids (dashed line) that barely oscillate. The respective frequency centroids can be found by

$$\omega_{1-C} = \frac{\int_{\omega<\omega_F} \omega I_\omega d\omega}{\int_{\omega<\omega_F} I_\omega d\omega}, \quad \omega_{2-C} = \frac{\int_{\omega>\omega_F} \omega I_\omega d\omega}{\int_{\omega>\omega_F} I_\omega d\omega}, \tag{9}$$

where $\omega_F = 2$ rad/fs.

B. Generation mechanism

Molecule states can be generated in different ways. Two possibilities are presented here. The most obvious one is the creation via direct superposition ($\delta = 0$), as mentioned before. This generation process is presented in Fig. 4 and has been detailed in [29] for two initial fundamental solitons

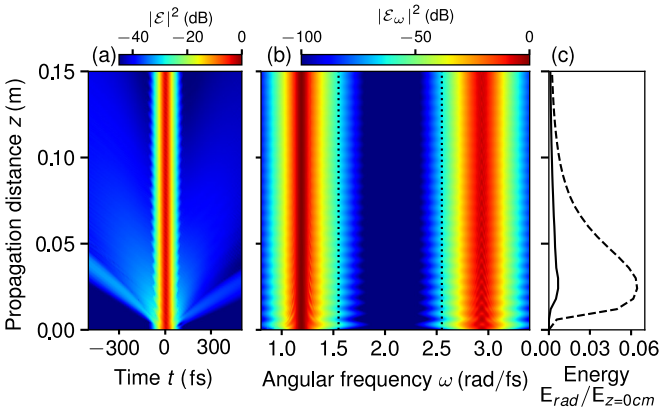

FIG. 4. Generation via direct superposition. Evolution is shown in (a) the time domain and (b) the frequency domain of two initial solitons with $\omega_1 = 1.2$ rad/fs, $\omega_2 = 2.939$ rad/fs, $t_{1,2} = 20$ fs, $N_{1,2} = 0.7$, and $\delta = 0$ fs. Dotted lines denote the location of the two ZDFs. (c) Energy E_{rad} of the emitted radiation during the formation process of the scenario in (a) and (b) (solid line) and of the scenario where $N_{1,2} = 1$ (dashed line).

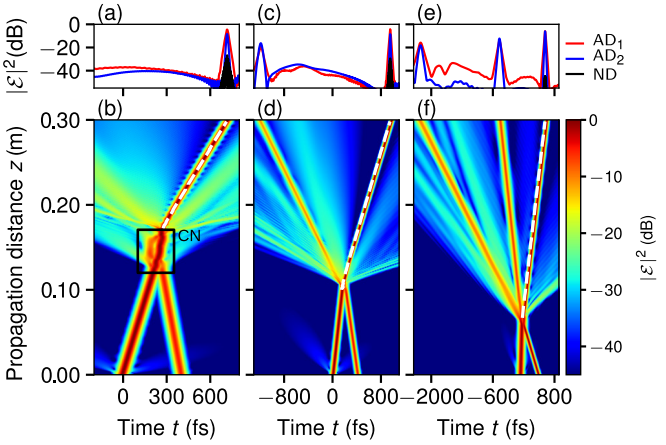

FIG. 5. Different soliton collision scenarios for the generation of soliton molecules: creation of (a) and (b) a single and (c)–(f) more molecule states. (a), (c), and (e) Temporal profiles are at $z = 30$ cm. The red, blue, and black lines denote the spectral parts in the dispersion regions AD_1, AD_2, and ND, respectively. The respective evolutions in the time domain are shown in (b), (d), and (f). A dashed line highlights the temporal trajectory of the most intense and shortest resulting molecule state. The black square in (b) highlights the transient compound nucleus.

(see Fig. 2 therein). Figures 4(a) and 4(b) show the evolution in the time and frequency domains, respectively, of two initially superimposed group-velocity-matched solitons of nonfundamental order ($N_{1,2} = 0.7$). The evolution of the energy of the emitted radiation during formation [Fig. 4(c)] is not significant compared with the situation where fundamental solitons ($N_{1,2} = 1.0$, dashed line) initiate the molecule formation. This observation underlines that for the generation of molecule states no fundamental solitons are necessary and that for this case less radiation is released.

Another possibility for the generation of two-frequency molecule states is the controlled collision process of two fundamental solitons. The evolution in the time domain of three different collision processes is presented in Fig. 5 with the initial parameters $t_{1/2} = 13.88/15$ fs and $\omega_{1,2} = 1.2/2.939$ rad/fs [Figs. 5(a) and 5(b)], $t_{1/2} = 15/15$ fs and $\omega_{1,2} = 1.2/2.939$ rad/fs [Figs. 5(c) and 5(d)], and $t_{1/2} = 25/15$ fs and $\omega_{1,2} = 1.2/2.97$ rad/fs [Figs. 5(e) and 5(f)]. For all cases shown the initial delay is $\delta = 400$ fs. Different parameters are intentionally chosen to demonstrate the generation of different molecule states. For example, adjusting the initial pulse duration of one of the soliton creates two molecule states in Fig. 5(d) compared to one in Fig. 5(b). Furthermore, an increase of the pulse duration of one of the initial solitons and an increased group-velocity mismatch can lead to the buildup of three molecule states. This underlines that the initial set of parameters has a strong influence on the final outcome.

On closer examination of the scenarios in Figs. 5(d) and 5(f), it can be seen that the generated molecules follow a specific order. The shortest and most intense states (dashed line) have the lowest group velocity, while states with higher pulse durations propagate faster. This order of ejection of the different molecule states is similar to the order of ejection of solitons in the soliton fission process [59,60]. The molecule creation process in Fig. 5(b) shows the collision of two solitons that interact over a non-negligible propagation distance (black square) before the actual molecule state emerges. In this transfer region, an intermediate state exists which is neither a soliton combination nor the final molecule state. This transient feature appears also in other fields such as nuclear physics where an intermediate state can form, namely, the compound nucleus [61]. In this analogy to a nuclear reaction involving, e.g., two nuclei, a large portion of their energy, mass, and angular momentum can be transferred between the interacting components, resulting in the transient formation of a compound nucleus.

A more detailed representation of the spectral energy distribution during the generation mechanism is presented in Table I. The energy E contributions of the initial solitons S_1 and S_2 and one of the resulting molecules (indicated by the dashed line) is calculated for each collision scenario. The respective total energy is defined by the sum of the input solitons. The energy content for the molecule state in ND decreases for the scenarios in Figs. 5(a)–5(c), which is also evident from the black line. The initial energy content in AD_1 decreases and increases in AD_2 from the example in Figs. 5(a)–5(c). Counterintuitively, the energy in the

TABLE I. Energy content (%) of different objects O, given by the initial solitons S_1, S_2, and the molecule M highlighted in Fig. 5. The energy distribution is given for the different regions of dispersion AD_1, AD_2, and ND.

	Fig. 5(a)			Fig. 5(b)			Fig. 5(c)		
O	AD_1	AD_2	ND	AD_1	AD_2	ND	AD_1	AD_2	ND
S_1	73.75	0	0	71.06	0	0	58.71	0	0
S_2	0	26.25	0	0	28.94	0	0	41.29	0
M	57.82	15.02	0.08	59.14	14.18	0.03	34.04	22.26	0

final molecule states exhibits the opposite behavior, indicating that more complex energy rearrangements do occur during generation. Table I shows a reduction in total energy owing to the formation of the molecule state, which is consistent with the well-known analogy of ordinary molecules, whose total energy is always less than the sum of the energy of the initial constituents. Moreover, the ratio of energy between the regions AD_1 and AD_2 before and after the collision process changes remarkably. This indicates that a large amount of energy is exchanged between the subpulses in AD_1 and AD_2, respectively. The various choices of initial solitons allow for control of the generation process to obtain a variety of different spectra, temporal properties, and number of generated states, while the resulting molecule states propagate in a stable manner.

C. Propagation dynamics under perturbation

The molecule states discussed above are asymptotically stable, allowing them to propagate unchanged over large distances. In this section we will introduce additional perturbations to investigate their impact on the propagation dynamics as well as to challenge the stability of these states. In particular, we will assess the effects of third-order dispersion and the Raman effect. Understanding the implications of such perturbations is crucial and is furthermore necessary for describing realistic systems and for practical applications.

1. Role of third-order dispersion

To better assess the impact of higher orders of dispersion on the dynamical evolution of two-frequency pulse compounds, we consider a simplified modeling approach that allows us to easily alter the dispersion characteristics of the individual subpulses. Therefore, we describe the propagation of a compound of two subpulses, represented by complex-valued slowly varying amplitudes $u \equiv u(z,\tau)$ and $v \equiv v(z,\tau)$, by coupled nonlinear Schrödinger equations [62] of the form

$$i\partial_z u - \frac{\beta_2'}{2}\partial_\tau^2 u + \gamma'(|u|^2 + 2|v|^2)u = i\frac{\beta_3'}{6}\partial_\tau^3 u, \quad \text{(10a)}$$

$$i\partial_z v - \frac{\beta_2}{2}\partial_\tau^2 v + \gamma(|v|^2 + 2|u|^2)v = i\frac{\beta_3}{6}\partial_\tau^3 v \quad \text{(10b)}$$

for propagation distance z and retarded time τ. The parameters are set to $\beta_2' = -0.222\ \mathrm{fs}^2/\mu\mathrm{m}$, $\gamma' = 0.450\ \mathrm{W}^{-1}/\mu\mathrm{m}$, $\beta_2 = -0.176\ \mathrm{fs}^2/\mu\mathrm{m}$, and $\gamma = 0.986\ \mathrm{W}^{-1}/\mu\mathrm{m}$, resembling the conditions under which the pulse compounds in Fig. 2 were generated. In Eqs. (10), β_3' and β_3 serve as tunable perturbation strengths. In addition to the nonlinear self-interaction of the individual pulses, Eqs. (10) include the mutual interaction of both subpulses through cross-phase modulation. Similar equations have been used as a basis to study two-soliton interactions in terms of a variational perturbation approach [63], superimposed solitons in birefringent fibers [64,65], coupled bright and dark pulses stabilized through cross-phase modulation [66,67], and soliton-radiation trapping in gas-filled hollow-core fibers [68].

The propagation equation (1) for the analytic signal can be reduced to the system of (10a) and (10b) under several simplifying assumptions and provided that both subpulses are separated by a vast frequency gap [46]. Above, the governing equation of either subpulse is perturbed by third-order dispersion. A nonzero value of β_3' introduces a zero-dispersion point at $\Omega_Z' = -\beta_2'/\beta_3'$ in Eq. (10a); so does β_3 for Eq. (10b). Considering a single nonlinear Schrödinger equation, such a perturbation enables the emission of resonant radiation by a soliton and affects its propagation dynamics through spectral recoil [48]. Here it allows us also to study how a perturbation of, say, subpulse v affects the entire pulse compound.

A clean moleculelike pulse compound for our subsequent numerical experiments is obtained by first considering two directly superimposed fundamental nonlinear Schrödinger solitons with duration $t_0 = 30$ fs, propagating under Eqs. (10) with $\beta_3' = \beta_3 = 0$. This initial condition separates into a moleculelike pulse compound and radiation. We then use the moleculelike pulse compound, free of additional radiation, as the starting point for a sequence of simulations with nonzero β_3' and β_3.

When modeling the interaction of vector solitons in birefringent fibers [69,70], third-order dispersion experienced by both subpulses is of the same sign. This is markedly different from the setting considered, wherein two pulses are coupled across a domain of normal dispersion, causing β_3' and β_3 to have different sign. Both situations are demonstrated in Fig. 6. As evident from Figs. 6(a) and 6(b), under the condition $\beta_3' = \beta_3 = 0.8\ \mathrm{fs}^3/\mu\mathrm{m}$, the zero-dispersion points will both be located at positive-frequency detunings, causing both pulses to experience a spectral recoil towards negative detunings. This results in positive leading-order corrections to their inverse group velocity. As a consequence, the pulses move towards positive times [Fig. 6(a)] and resonant radiation is generated at $\Omega_R' \approx 0.8$ rad/fs and $\Omega_R \approx 0.7$ rad/fs [Fig. 6(b)]. In contrast to this, as shown in Figs. 6(c) and 6(d), under the condition $\beta_3' = -\beta_3 = 0.8\ \mathrm{fs}^3/\mu\mathrm{m}$, the zero-dispersion points will be on opposite sides of the spectrum. As a result, the leading-order corrections to the inverse group velocities of the free subpulses would naturally be of different sign. The mutual binding between the pulses counteracts this free behavior, resulting in a partly canceled group-velocity shift of the entire compound. This becomes apparent when comparing Figs. 6(a) and 6(c). In this case, resonant radiation is generated at $\Omega_R' \approx 0.8$ rad/fs and $\Omega_R \approx -0.7$ rad/fs.

To get a better understanding of the impact of nonequal third-order dispersion on the dynamics of a pulse compound, we next perform a sequence of simulations for $\beta_3' = 0$ and nonzero β_3, i.e., we deliberately perturb only Eq. (10b) by third-order dispersion. In Fig. 7(a) we show the dynamical evolution of the subpulse intensities $|u|^2$ and $|v|^2$ for one such simulation run using $\beta_3 = -0.8\ \mathrm{fs}^3/\mu\mathrm{m}$. We also show the corresponding centroid trajectories $t_1 = \int \tau|u|^2 d\tau / \int |u| d\tau$ and $t_2 = \int \tau|v|^2 d\tau / \int |v| d\tau$ for different perturbation strengths. As evident from these trajectories, nonzero β_3 results in increased (decreased) velocity of the *entire* pulse compound when $\beta_3 < 0$ ($\beta_3 > 0$). This clearly highlights the cross-phase-modulation-induced binding between both pulses already recognized in Fig. 6(c): Subpulse u, which is not directly affected by the perturbation, is dragged along with v. In Fig. 7(b) we show the variation of the subpulse separation $\xi = t_1 - t_2$ upon propagation, indicating the internal dynamics of the pulse compounds for nonzero β_3. The internal dynamics for similar pulse compounds, reminiscent

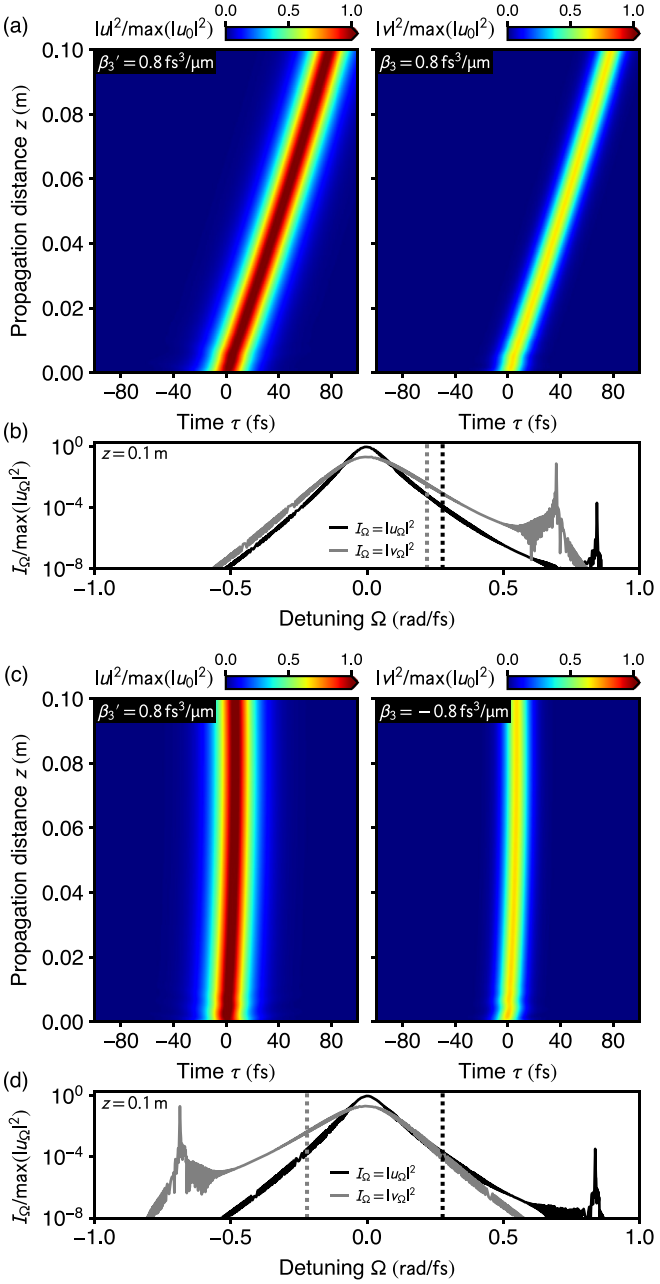

FIG. 6. Impact of third-order dispersion on the propagation dynamics of pulse compounds, modeled via coupled nonlinear Schrödinger equations. (a) Dynamics of both subpulses subject to the same value of third-order dispersion $\beta_3' = \beta_3 = 0.8\ \mathrm{fs}^3/\mu\mathrm{m}$. (b) Subpulse spectra at propagation distance $z = 0.1$ m. Dashed lines indicate zero-dispersion points at $\Omega_Z' \approx 0.277$ rad/fs and $\Omega_Z \approx 0.220$ rad/fs. (c) and (d) Same as (a) and (b) but for $\beta_3' = -\beta_3 = 0.8\ \mathrm{fs}^3/\mu\mathrm{m}$. Dashed lines indicate zero-dispersion points at $\Omega_Z' \approx 0.277$ rad/fs and $\Omega_Z \approx -0.220$ rad/fs.

of molecular vibrations, were reported previously [29,46]. For a given value of β_3, ξ exhibits a damped oscillatory motion decaying proportionally to $\exp(-z/z_0)$. For example, in the case of $\beta_3 = \pm 0.8\ \mathrm{fs}^3/\mu\mathrm{m}$ we find $z_0 \approx 0.0042$ m. We further determined the integrated energy flux of the dispersive waves radiated off by the pulse component v ac-

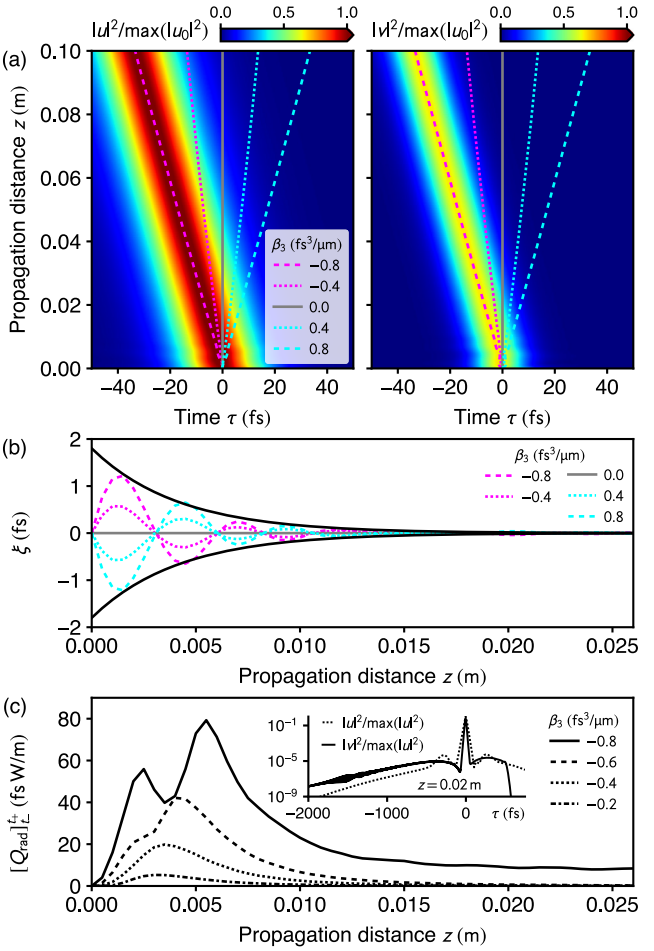

FIG. 7. Impact of third-order dispersion acting on a single subpulse. (a) Dynamical evolution of subpulse intensities $|u|^2$ (left) and $|v|^2$ (right) for $\beta_3 = -0.8\ \mathrm{fs}^3/\mu\mathrm{m}$. Lines indicate centroid trajectories t_1 (for u) and t_2 (for v) for different values of β_3. Third-order dispersion is included in the governing equation for v only (see the text). (b) Variation of subpulse separation $\xi = t_1 - t_2$ upon propagation for different values of β_3. (c) Integrated energy flux $[Q_{\mathrm{rad}}]_{t_-}^{t_+}$, with $t_\pm = t_2 \pm 100$ fs, leaving pulse component v upon propagation for different perturbation strengths. The inset shows intensities of localized pulses and generated radiation for $\beta_3 = -0.6\ \mathrm{fs}^3/\mu\mathrm{m}$ at $z = 0.02$ m.

cording to [48]

$$[Q_{\mathrm{rad}}]_{t_-}^{t_+} = -\partial_z \int_{t_-}^{t_+} |v|^2 d\tau \tag{11}$$

for $t_\pm = t_2 \pm 100$ fs, which is shown in Fig. 7(c) for different perturbation strengths. We find that the majority of energy, which is converted to dispersive waves, leaves the soliton over a propagation length that agrees well with the decay length z_0 of the damped oscillatory motion of ξ. Hence, a possible explanation for the dampening mechanism is provided by the emission of dispersive waves by both subpulses [see the inset in Fig. 7(c)], especially during the initial propagation stage, consistent with previous observations [29,46].

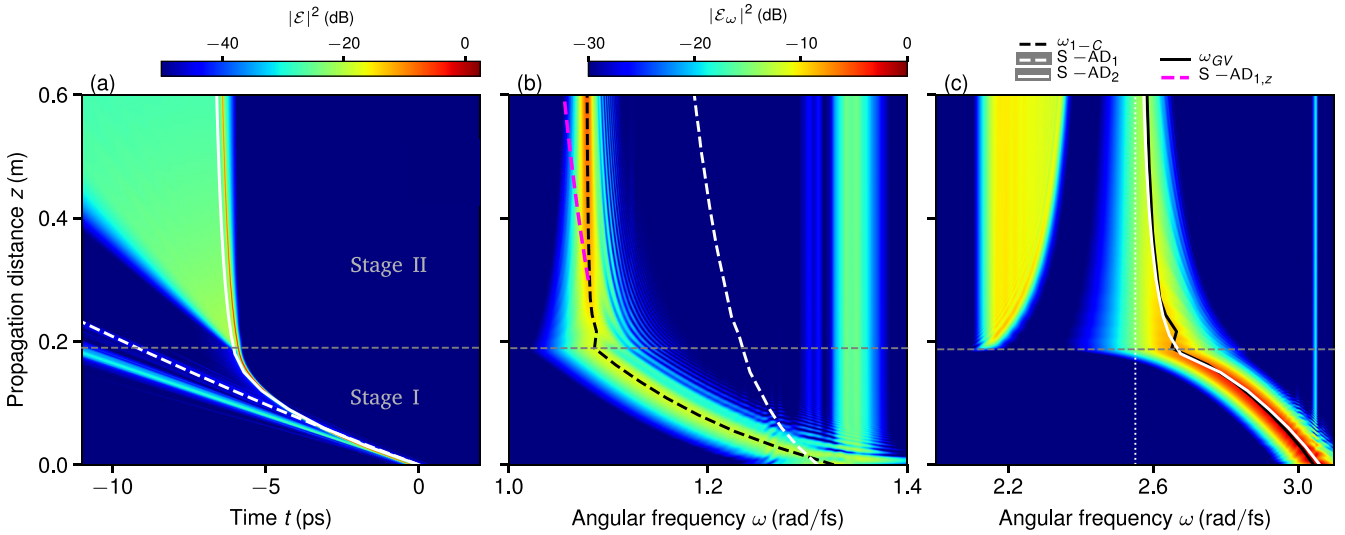

FIG. 8. Impact of the Raman effect on compound with stronger constituent in AD_2. White solid and dashed lines indicate trajectories of associated solitons $\mathsf{S}-\mathsf{AD}_1$ and $\mathsf{S}-\mathsf{AD}_2$ with fitted parameters $t_1 = 18$ fs at $\omega_1 = 1.31$ rad/fs and $t_2 = 19$ fs at $\omega_1 = 3.06$ rad/fs, respectively. (a) Dynamical evolution in the time domain. The reference frame moves with velocity $v_{\mathrm{ref}} = v_g(\omega_0 = 2.55\ \mathrm{rad/fs})$. (b) and (c) Evolution in the frequency domain. In (b) the black dashed line (labeled ω_{1-C}) indicates the frequency centroid of the subpulse. The pink dashed line $\mathsf{S}-\mathsf{AD}_{1,z}$ shows the trajectory of a further associated soliton at $z \approx 0.3$ m. In (c) the black solid line (labeled ω_{GV}) indicates the frequency group-velocity matched to ω_{1-C}. The vertical dotted line indicates zero-dispersion frequency ω_{Z2}. The horizontal gray dashed line marks the distance at which energy transfer to the region of normal dispersion sets in.

Our investigation shows the impact that β_3 has on the individual subpulses as well as the complete compound when its sign or value differs. We demonstrate that different β_3 values impose a different group velocity on the subpulses, but a stable propagation of the molecule state is ensured as a result of the strong mutual binding between the constituents.

2. *Raman effect*

Depending on the system where the bound states are created, the effect of Raman scattering resulting from inelastic scattering of a photon at atoms and molecules has to be taken into account. For example, in the propagation dynamics for a soliton in nonlinear fibers this leads to a self-frequency shift (SFS) [71]. Here we show that the Raman effect counteracts the inherent binding mechanism and offers the possibility for a better understanding of the mutual interaction between the two constituents. The impact of Raman scattering on nonlinearly coupled solitons has been investigated for vector solitons inside birefringent optical fibers for a dispersion profile with a ZDF on the shorter-wavelength [69,70] as well as on the longer-wavelength side [72] of the vector solitons. For the case where the ZDF is located on the longer-wavelength side, no remarkable effect of the Raman effect is observed as the frequencies of both solitons are shifted away from the ZDF. For the opposite case, both pulses are subject to the recoil effect [48].

Here the slopes of the group-velocity dispersion at the frequencies associated with both constituents of a compound state have a different sign [see Fig. 1(b)]. Due to this opposite sign of the β_3 coefficients for the two constituents, peculiar conditions for the compound state are given in our system. Since for pulses in AD_1 the ZDFs lie at higher frequencies, a fundamental soliton in this region would propagate under a continuous SFS [71]. In contrast, a fundamental soliton in AD_2 is subject to the recoil effect [73] when approaching a ZDF, as usually seen for fiber profiles with one region of anomalous dispersion [74]. Consequently, we have a strong counteracting mechanism on the constituents of the molecule state in our system.

Figure 8 shows the propagation of a molecule under the impact of the Raman effect for the case where the subpulse located in AD_1 is weaker than the one in AD_2. The propagation dynamics can be divided into two stages I and II. The initial molecule state is different from the example used for previous investigations. Here it is important that both subpulses are clearly distinguishable to allow for an approximation with fundamental solitons at best. For this reason, broader initial pulse durations are advisable. In stage I a continuous deceleration due to the SFS occurs up to a point where there is an abrupt cancellation of the SFS (stage II) and a recoil effect sets in, accompanied by the generation of radiation. The evolution in the time domain [Figs. 8(a)] is shown in the reference frame with the velocity $v_{\mathrm{ref}} = v_g(\omega_0 = 2.55\ \mathrm{rad/fs})$. By choosing this velocity the resulting pulse in stage II appears stationary. The first important observation is that the molecule does not dissolve into its constituents, although the strength of the Raman effect on the constituents is different, being dependent on the differences of the temporal and spectral widths. Note that only the center frequency of one of the constituents is shifted towards a ZDF and that we have three different temporal durations characterizing one compound state. The temporal evolution also reveals that the duration of the molecule state changes with ongoing propagation. Frequency shifts induce also a change in the temporal properties [37,38,44,51]. Here it leads to a compression for the subpulse in AD_2 down to approximately 7 fs where stage II sets in. This results also in

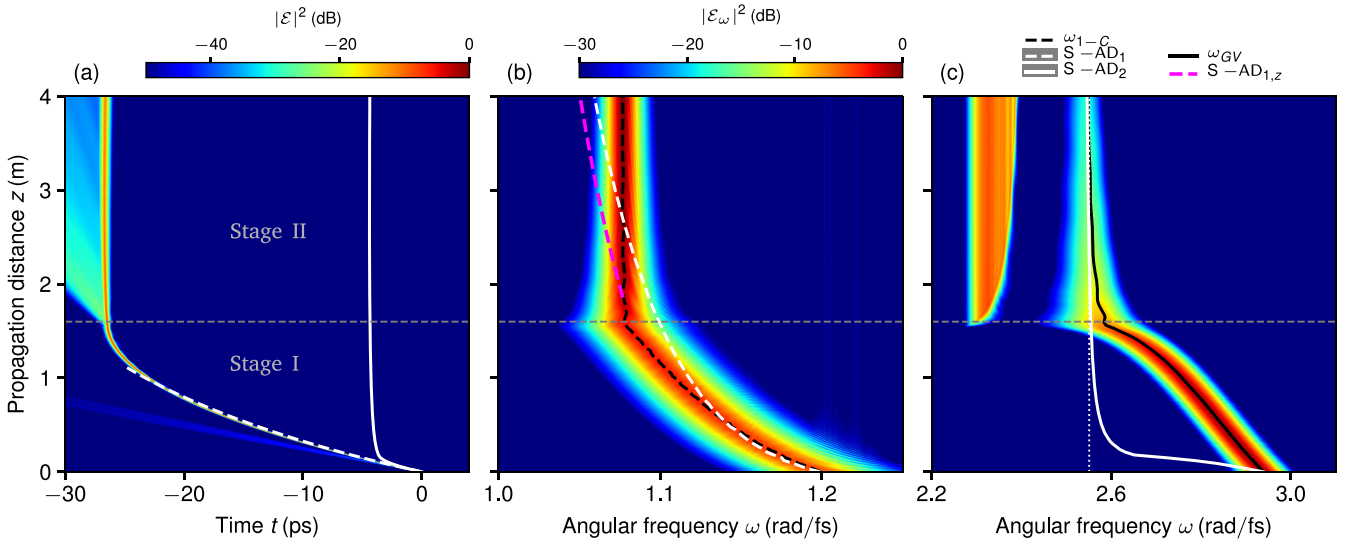

FIG. 9. Impact of the Raman effect on the compound with a stronger constituent in AD_1. White solid and dashed lines indicate trajectories of associated solitons $\mathsf{S}-\mathsf{AD}_1$ and $\mathsf{S}-\mathsf{AD}_2$ with fitted parameters $t_1 = 33$ fs at $\omega_1 = 1.2$ rad/fs and $t_2 = 20$ fs at $\omega_1 = 2.939$ rad/fs, respectively. (a) Dynamical evolution in the time domain. The reference frame moves with velocity $v_{\mathrm{ref}} = v_g(\omega_0 = 2.55\ \mathrm{rad/fs})$. (b) and (c) Evolution in the frequency domain. In (b) the black dashed line (labeled ω_{1-C}) indicates the frequency centroid of the subpulse. The pink dashed line $\mathsf{S}-\mathsf{AD}_{1,z}$ shows the trajectory of a further associated soliton at $z \approx 2$ m. In (c) the black solid line (labeled ω_{GV}) indicates the frequency group-velocity matched to ω_{1-C}. The vertical dotted line indicates zero-dispersion frequency ω_{Z2}. The horizontal gray dashed line marks the distance at which energy transfer to the region of normal dispersion sets in.

a temporal compression for the entire compound at this point. With ongoing propagation, although there is no frequency shift, the molecule state broadens because the remaining pulse changes its properties due to the depletion of the binding partner. The trajectory of the frequency centroid ω_{1-C} for the constituent in AD_1 is highlighted by a black dashed line in Fig. 8(b). A black solid line in Fig. 8(c) shows ω_{GV}, i.e., the frequency group-velocity matched to ω_{1-C}. An uniform frequency downshift for both subpulses occurs until the frequency of the stronger constituent in AD_2 reaches the ZDF and stage II initiates. The subpulse accumulates in the vicinity of the ZDF due to the spectral recoil effect [73] and energy is steadily shifted to the region of normal dispersion. We observe that this has an immediate powerful effect on the weaker subpulse in AD_1: Although there is no ZDF barrier for this subpulse, its center frequency shift is canceled as well [Fig. 8(b)].

Next we will facilitate intuition on how the above effects affect each subpulse. We first perform an additional numerical experiment for each subpulse, clarifying the propagation dynamics of a fundamental soliton with duration and center frequency that match those of the subpulse at $z = 0$ m. Below, for brevity, we refer to such a specially tailored fundamental soliton as an associated soliton. The frequency centroids of these associated solitons are included as white dashed and solid lines in Figs. 8(a)–8(c). Comparing their frequency centroids to the actual subpulse spectra, we find excellent agreement for the strong subpulse [Fig. 8(c)] and large deviations for the weak subpulse [Fig. 8(b)]. Since for the chosen parameters the larger part of the spectral energy in this scenario is located in AD_2, it is exactly this subpulse that determines the behavior of the other one. Indeed, both subpulses remain group-velocity matched. This is evident from Fig. 8(c), where ω_{GV}, i.e., the frequency group-velocity matched to ω_{1-C}, is included. This strong self-preservation, supported by the inherent binding mechanism of the soliton molecule, leads to a stable decelerated propagation of the state [Fig. 8(a)]. The resulting group velocity is determined by the stronger subpulse, approaching the ZDF. With further propagation in stage II, energy is transferred into region ND and the energy of the strong subpulse is reduced. Nevertheless, the binding between the two constituents is strong enough to allow the existence of a molecule state.

The second example is chosen in such a way that the subpulse in AD_1 is dominant. Thus, we can investigate what happens if the stronger subpulse does not meet any ZDF. The evolution in the time and frequency domains is shown in Figs. 9(a), 9(b) and 9(c), respectively. At first, similar to the preceding case, the strength of the shift is dominated by the stronger subpulse (which is now located in AD_1). Note that the subpulse in AD_2 exhibits a much smaller temporal duration and its associated soliton achieves a much stronger deceleration [see Fig. 9(c)]. As above, there is an abrupt cancellation of the frequency shift for both pulses in stage II. This time, however, the change is induced by the weaker pulse. Surprisingly, we still observe the existence of a molecule state with further propagation. The stronger pulse does not directly dissolve from the molecule state and the frequency centroids of both subpulses remain group-velocity matched, determined by the velocity close to the ZDF for the weaker pulse in AD_2. For comparison, we plot the trajectories of associated solitons in Figs. 9(b) and 9(c). In addition, we provide the trajectories for yet another associated soliton, modeled after the strong

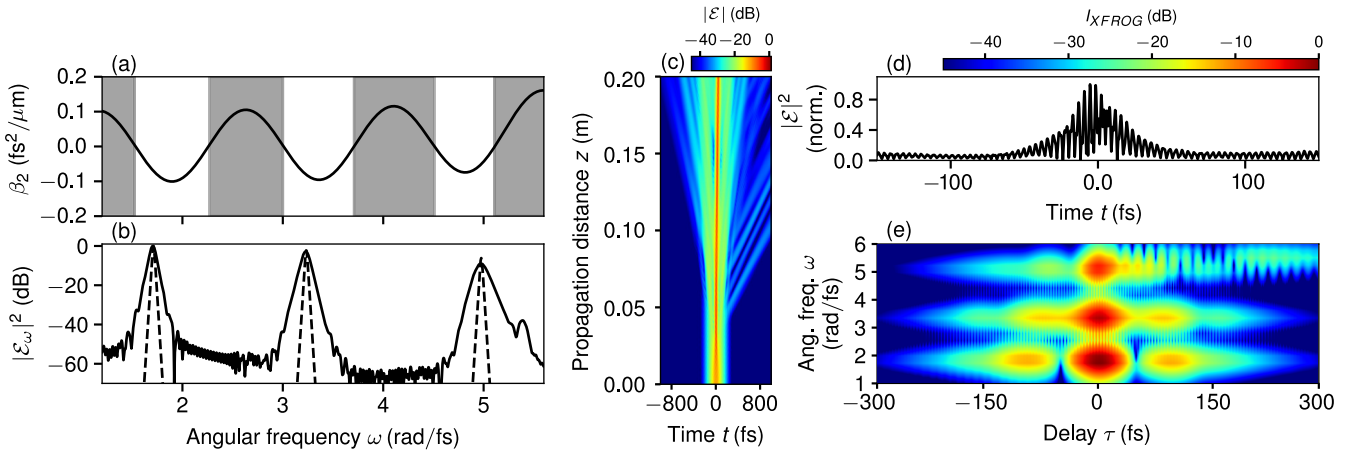

FIG. 10. Generation process of a molecule state with three subpulses. (a) Group-velocity dispersion (GVD) curve that exhibits three domains of anomalous dispersion and allows for group-velocity-matched propagation of three frequencies at which GVD is anomalous. Domains of normal dispersion are shaded gray. (b) Spectra at $z = 0$ cm (dashed line) and $z = 20$ cm (solid line). The latter shows the triplet state, including any accompanying radiation. (c) Evolution in the time domain. (d) Time-domain intensity and (e) spectrogram at $z = 20$ cm for $\sigma = 40$ fs in Eq. (8).

subpulse at a z position within stage II, where the energy shift to the region of normal dispersion has set in already [pink line in Fig. 9(b)].

Due to the recoil effect, the weaker pulse radiates and transfers energy to the normal dispersion regime, leading to a slow depletion of one of the constituents of the bound state. The depletion of the binding partner occurs steadily and for very large propagation distances, the bound state eventually dissolves. We find that the remaining subpulse, i.e., the one in AD_1, forms a fundamental soliton which is now under the usual influence of a SFS (not shown).

As in Refs. [69,72], we observe that the Raman effect is not detrimental to the copropagation of temporally locked pulses. Although in our systems the competition between the binding mechanism and Raman effect is quite distinctive, as the underlying conditions provide a strong counteracting interaction between the subpulses, a molecule state is supported despite a strong perturbation. Our analysis of the two simple examples above provides a deeper understanding of the molecule state and the strength of cohesion displayed by its constituents. Our approach for investigation of the bound state relies on the interpretation of two pulses with well-separated spectra, with a binding mechanism provided by incoherent XPM. Let us note that the dynamics of the molecule states can be much more complicated, e.g., forming an oscillating compound state or a state with a spectrum reaching over the normal dispersion regime. To thoroughly characterize the effect of Raman scattering on such molecule states as well, further investigations and complementary approaches of analysis are necessary. Nevertheless, our simple picture reveals intriguing dynamics, such as the cancellation of the self-frequency shift for the entire pulse compound, even though just one of its constituents approaches a zero-dispersion point. This appears directly interesting for applications, as the properties for one pulse can be transferred to another pulse over a wide gap in the spectrum.

D. Molecule states with three subpulses

Three-soliton molecules, i.e., bound states consisting of three solitons, have been demonstrated in dispersion-managed fibers [75]. More recently, polychromatic soliton molecules with up to three frequencies, i.e., three-color soliton molecules, have been studied in theory and experiment for a mode-locked laser cavity [31]. Such a concept has even been expanded to spectrally periodic structures.

Here we transfer the concept of such multicolor compound states to the presented framework. To support a moleculelike bound state with three distinct subpulses in our system, a propagation constant is needed that allows for group-velocity matching of three distinct frequencies for which group-velocity dispersion is anomalous. A representative group-velocity dispersion profile satisfying these requirements is shown in Fig. 10(a). It exhibits multiple separate domains of anomalous dispersion. Based on the underlying propagation constant, the generation process of a molecule state with three distinct subpulses, subsequently referred to as a triplet state, is shown in Fig. 10(c). Therefore, three fundamental solitons with durations $t_1 = t_2 = t_3 = 60$ fs and center frequencies $\omega_1 = 1.711$ rad/fs, $\omega_2 = 3.233$ rad/fs, and $\omega_3 = 4.976$ rad/fs are initially superimposed and propagated using Eq. (1). Similar to the generation process of two-frequency pulse compounds discussed above, this results in a localized state as well as additional radiation. Here the localized state now exhibits three distinct subpulses.

Upon propagation, an increase in peak intensity and a decrease in the duration of the localized state, resulting from the mutual interaction between the three subpulses, are clearly visible [Fig. 10(c)]. Figure 10(b) shows the spectrum of the triplet state at $z = 20$ cm (solid line). In comparison to the initial spectrum (dashed line), strong spectral broadening of the initial pulses is evident. A spectrogram of the field at $z = 20$ cm is shown in Fig. 10(e), highlighting the tripartite

structure of the localized state in the time-frequency plane. All three subpulses exhibit similar intensities. The simultaneous presence of several frequencies is also reflected by the highly fringed appearance of the time-domain intensity shown in Fig. 10(d). From this figure it can also be seen that the duration of the triplet state is much shorter than any initial soliton; we estimate its duration to be approximately equal to 19 fs.

IV. CONCLUSION

We have performed numerical simulations to investigate the properties of heteronuclear two-color soliton molecules. We characterized the rearrangement and final distribution of energy among the constituents of such molecules for two different generation mechanisms, which allowed us to draw connections between the contributing parameters as well as to gain insight into the highly dynamic molecule generation process.

We further discussed the impact of different types of perturbation on the molecule states. We assessed the role of third-order dispersion in terms of a simplified modeling approach, wherein molecule states are described via coupled nonlinear Schrödinger equations. Perturbing only a single subpulse by third-order dispersion, we found that the entire pulse compound is affected. This highlights the cross-phase-modulation-induced binding between the constituents of a molecule, enabling both its constituents to remain group-velocity matched despite perturbations. Studying the impact of the Raman effect, we found that this mutual binding results in astounding dynamics of the molecule states: The self-frequency shift of the entire pulse compound is canceled, even though only one of its subpulses approaches a zero-dispersion point and so experiences a spectral recoil. Furthermore, this behavior is independent of whether the stronger or weaker subpulse is constrained by the zero-dispersion point. An investigation of these perturbations revealed that the constituent subpulses of the molecule state are strongly connected. Changes imposed on one subpulse individually are transferred to the second one over a large frequency gap and influence the propagation dynamics of the entire inseparable compound.

Finally, we transferred the concept of multicolor molecule states to the system presented herein, by showing how a molecule state with three subpulses can be realized by means of an adequate propagation constant. This underlines the flexibility of the system, limited only by the choice of the propagation constant. This opens up the possibility to generate molecule states with many constituents as well as generation mechanisms for very broad and bright spectra, possibly with supercontinuum properties.

ACKNOWLEDGMENTS

The authors acknowledge financial support from Deutsche Forschungsgemeinschaft (Projects No. BA4156/4-2 and No. MO 850-20/1) under Germany's Excellence Strategy within the Clusters of Excellence PhoenixD (Photonics, Optics, and Engineering—Innovation Across Disciplines) (EXC 2122, Project No. 390833453) and QuantumFrontiers (EXC 2123, Project No. 390837967).

[1] P. G. Drazin and R. S. Johnson, *Solitons: An Introduction* (Cambridge University Press, Cambridge, 1989).
[2] Y. S. Kivshar and G. P. Agrawal, *Optical Solitons: From Fibers to Photonic Crystals* (Academic, San Diego, 2003).
[3] A. V. Gurevich, *Nonlinear Phenomena in the Ionosphere* (Springer, Berlin, 1978).
[4] R. Balakrishnan, Phys. Rev. A **32**, 1144 (1985).
[5] G. I. Stegeman and M. Segev, Science **286**, 1518 (1999).
[6] F. Mitschke, *Fiber Optics: Physics and Technology* (Springer, Berlin, 2010).
[7] H. A. Haus and W. S. Wong, Rev. Mod. Phys. **68**, 423 (1996).
[8] N. J. Zabusky and M. D. Kruskal, Phys. Rev. Lett. **15**, 240 (1965).
[9] M. N. Islam, C. D. Poole, and J. P. Gordon, Opt. Lett. **14**, 1011 (1989).
[10] M. Stratmann, T. Pagel, and F. Mitschke, Phys. Rev. Lett. **95**, 143902 (2005).
[11] A. Hause, H. Hartwig, M. Böhm, and F. Mitschke, Phys. Rev. A **78**, 063817 (2008).
[12] A. V. Buryak and N. N. Akhmediev, Phys. Rev. E **51**, 3572 (1995).
[13] B. A. Malomed, Phys. Rev. E **47**, 2874 (1993); B. A. Malomed, A. Zavyalov, R. Iliew, O. Egorov, and F. Lederer, Phys. Rev. A **80**, 043829 (2009).
[14] I. Oreshnikov, R. Driben, and A. Yulin, Phys. Rev. A **96**, 013809 (2017).
[15] N. N. Akhmediev, A. Ankiewicz, and J. M. Soto-Crespo, Phys. Rev. Lett. **79**, 4047 (1997).
[16] M. Haelterman, S. Trillo, and P. Ferro, Opt. Lett. **22**, 84 (1997).
[17] W. Weng, R. Bouchand, E. Lucas, E. Obrzud, T. Herr, and T. J. Kippenberg, Nat. Commun. **11**, 2402 (2020).
[18] D. Neshev, E. Ostrovskaya, Y. Kivshar, and W. Krolikowski, Opt. Lett. **28**, 710 (2003).
[19] V. V. Afanasjev and V. A. Vysloukh, J. Opt. Soc. Am. B **11**, 2385 (1994).
[20] E. N. Tsoy and F. K. Abdullaev, Phys. Rev. E **67**, 056610 (2003).
[21] B. A. Umarov, N. A. B. Aklan, B. B. Baizakov, and F. K. Abdullaev, J. Phys. B **49**, 125307 (2016).
[22] Z. Chen, M. Acks, E. A. Ostrovskaya, and Y. S. Kivshar, Opt. Lett. **25**, 417 (2000).
[23] Y. V. Kartashov, L. C. Crasovan, D. Mihalache, and L. Torner, Phys. Rev. Lett. **89**, 273902 (2002).
[24] G. Xu, A. Gelash, A. Chabchoub, V. Zakharov, and B. Kibler, Phys. Rev. Lett. **122**, 084101 (2019).
[25] X. Liu, X. Yao, and Y. Cui, Phys. Rev. Lett. **121**, 023905 (2018).
[26] K. Krupa, K. Nithyanandan, U. Andral, P. Tchofo-Dinda, and P. Grelu, Phys. Rev. Lett. **118**, 243901 (2017).

[27] U. Al Khawaja and A. Boudjemaa, Phys. Rev. E **86**, 036606 (2012).
[28] P. Grelu and N. Akhmediev, Nat. Photon. **6**, 84 (2012).
[29] O. Melchert, S. Willms, S. Bose, A. Yulin, B. Roth, F. Mitschke, U. Morgner, I. Babushkin, and A. Demircan, Phys. Rev. Lett. **123**, 243905 (2019).
[30] K. K. K. Tam, T. J. Alexander, A. Blanco-Redondo, and C. M. de Sterke, Phys. Rev. A **101**, 043822 (2020).
[31] J. P. Lourdesamy, A. F. J. Runge, T. J. Alexander, D. D. Hudson, A. Blanco-Redondo, and C. M. de Sterke, Nat. Phys. **18**, 59 (2022).
[32] G. Moille, Q. Li, S. Kim, D. Westly, and K. Srinivasan, Opt. Lett. **43**, 2772 (2018).
[33] O. Melchert, A. Yulin, and A. Demircan, Opt. Lett. **45**, 2764 (2020).
[34] A. Ferrando, E. Silvestre, J. J. Miret, and P. Andres, Opt. Lett. **25**, 790 (2000).
[35] L. Zhang, Q. Lin, Y. Yue, Y. Yan, R. G. Beausoleil, and A. E. Willner, Opt. Express **20**, 1685 (2012).
[36] S. Roy and F. Biancalana, Phys. Rev. A **87**, 025801 (2013).
[37] A. Demircan, S. Amiranashvili, C. Brée, and G. Steinmeyer, Phys. Rev. Lett. **110**, 233901 (2013).
[38] A. Demircan, S. Amiranashvili, C. Brée, C. Mahnke, F. Mitschke, and G. Steinmeyer, Sci. Rep. **2**, 850 (2012).
[39] D. V. Skryabin and A. V. Gorbach, Rev. Mod. Phys. **82**, 1287 (2010).
[40] C. M. de Sterke, Opt. Lett. **17**, 914 (1992).
[41] T. G. Philbin, C. Kuklewicz, S. Robertson, S. Hill, F. König, and U. Leonhardt, Science **319**, 1367 (2008).
[42] D. Faccio, Contemp. Phys. **53**, 97 (2012).
[43] B. W. Plansinis, W. R. Donaldson, and G. P. Agrawal, Phys. Rev. Lett. **115**, 183901 (2015).
[44] A. Demircan, S. Amiranashvili, C. Brée, U. Morgner, and G. Steinmeyer, Opt. Lett. **39**, 2735 (2014).
[45] A. Demircan, S. Amiranashvili, and G. Steinmeyer, Phys. Rev. Lett. **106**, 163901 (2011).
[46] O. Melchert, S. Willms, U. Morgner, I. Babushkin, and A. Demircan, Sci. Rep. **11**, 11190 (2021).
[47] O. Melchert and A. Demircan, Opt. Lett. **46**, 5603 (2021).
[48] N. Akhmediev and M. Karlsson, Phys. Rev. A **51**, 2602 (1995).
[49] P. Beaud, W. Hodel, B. Zysset, and H. Weber, IEEE J. Quantum Electron. **23**, 1938 (1987).
[50] M. Conforti, C. Mas Arabi, A. Mussot, and A. Kudlinski, Opt. Lett. **42**, 4004 (2017).
[51] A. Demircan, S. Amiranashvili, C. Brée, C. Mahnke, F. Mitschke, and G. Steinmeyer, Appl. Phys. B **115**, 343 (2014).
[52] A. Demircan, S. Amiranashvili, C. Brée, U. Morgner, and G. Steinmeyer, Opt. Express **22**, 3866 (2014).
[53] S. Amiranashvili and A. Demircan, Phys. Rev. A **82**, 013812 (2010).
[54] S. Amiranashvili and A. Demircan, Adv. Opt. Technol. **2011**, 989515 (2011).
[55] O. Melchert, U. Morgner, B. Roth, I. Babushkin, and A. Demircan, in *Computational Optics II*, edited by D. G. Smith, F. Wyrowski, and A. Erdmann, SPIE Proc. Vol. 10694 (SPIE, Bellingham, 2018).
[56] O. Melchert and A. Demircan, Comput. Phys. Commun. **273**, 108257 (2022).
[57] J. C. Butcher, *The Numerical Analysis of Ordinary Differential Equations: Runge-Kutta and General Linear Methods* (Wiley, Chichester, 1987).
[58] O. Melchert, B. Roth, U. Morgner, and A. Demircan, SoftwareX **10**, 100275 (2019).
[59] A. V. Husakou and J. Herrmann, Phys. Rev. Lett. **87**, 203901 (2001).
[60] A. Demircan and U. Bandelow, Appl. Phys. B **86**, 31 (2006).
[61] K. Bethge, G. Walter, and B. Wiedemann, *Kernphysik: Eine Einführung* (Springer, Berlin, 2007).
[62] G. P. Agrawal, *Nonlinear Fiber Optics*, 4th ed. (Academic, San Diego, 2007).
[63] D. Anderson and M. Lisak, Phys. Scr. **33**, 193 (1986).
[64] T. Ueda and W. L. Kath, Phys. Rev. A **42**, 563 (1990).
[65] C. R. Menyuk, J. Opt. Soc. Am. B **5**, 392 (1988).
[66] V. V. Afanas'ev, E. M. Dianov, A. M. Prokhorov, and V. N. Serkin, Pis'ma Zh. Eksp. Teor. Fiz. **48**, 588 (1988). [JETP Lett. **48**, 638 (1988)].
[67] S. Trillo, S. Wabnitz, E. M. Wright, and G. I. Stegeman, Opt. Lett. **13**, 871 (1988).
[68] M. F. Saleh and F. Biancalana, Phys. Rev. A **87**, 043807 (2013).
[69] P. Balla and G. P. Agrawal, Phys. Rev. A **98**, 023822 (2018).
[70] P. Balla and G. P. Agrawal, J. Opt. Soc. Am. B **35**, 2302 (2018).
[71] F. M. Mitschke and L. F. Mollenauer, Opt. Lett. **11**, 659 (1986).
[72] V. Mishra and S. K. Agrawal, J. Opt. Soc. Am. B **36**, 1806 (2019).
[73] D. V. Skryabin, F. Luan, J. C. Knight, and P. S. J. Russel, Science **301**, 1705 (2003).
[74] J. H. Lee, J. van Howe, C. Xu, and X. Liu, IEEE J. Sel. Top. Quantum Electron. **14**, 713 (2008).
[75] P. Rohrmann, A. Hause, and F. Mitschke, Phys. Rev. A **87**, 043834 (2013).